Simulating the Behaviour of Charged Particles in a Penning Trap

Kim Dahl-Hansen, Fridtjof Ronge Gjengset,
Sebastian Ranum Tenmann & Cecilie Klarpås
(Dated: October 27, 2021)

This paper aimed to explore advantages and limitations in numerically simulating a Penning trap. We analytically and numerically solved the equations of motion for particles inside a penning-trap and performed an error analysis to determine the precision of our numerical model. We successfully created a numerical model using equations of motion based on Newton's second law and Coulomb's law, using a 4th order Runge-Kutta algorithm. Our simulation exhibited the expected oscillatory and rotational movement as predicted from the Lorentz force. Furthermore, our code showed the more chaotic nature when including inter-particle interactions. Our relative error using 4th order Runge-Kutta was in the interval $[10^{-10}, 10^{-1}]$ dependent on the step-size, dramatically better than simpler methods we compared with. In further investigation we collected data on particle ejection in larger groups of particles, showing as expected that even though many escape, there are some left within the trap. [a]

I. INTRODUCTION

In many areas of research it is necessary to trap and transport particles. This however can be problematic if the particle interacts with ordinary matter (as for instance antimatter that will annihilate when meeting ordinary matter). One way of overcoming this potential issue is to use a Penning trap. In addition, this form of storing charged particles/ions can also be used to determine their respective masses by analysing their movement within the trap[2]. Penning traps use static magnetic and electric fields to confine charged particles by limiting the motion in each direction. The electric field limits motion in the z-direction, while the magnetic field imposed in the z-direction limits the motion in the xy-plane by forcing the particles into orbital motion. The result is that the particle is trapped.

With this project we aimed to do a numerical investigation into the effects of such a Penning trap on charged particles, given different conditions. Our code performs simulations of the system, which can be used to see how various initial conditions effect the particles before a physical experiment is conducted. We tested our code by running it for a single particle, and checked the motion and error compared to what was expected. Then, we explored our code by introducing a second particle and computed their motion when their interactions were neglected and when they were accounted for. Finally we changed the physical parameters of the trap and filled with with 100 particles and imposed a time-varying EM-field in order to investigate the resonance behaviour of the system. The results were then compared and presented as graphs.

In our setup the system is dependent on both the positions and the velocities of the particles involved, giving coupled equations guiding the evolution. For this reason we chose to utilize the 4th order Runge-Kutta algorithm, which uses four estimates of the gradient in each interval. This was justified further, as it produced a smaller error than similar algorithms, with a local error of h^5 and global error of h^4[1] while still using a larger step-size, giving a more effective code.

We have neglected the quantum aspects of the trap, and assumed the trap to be ideal system where the electric field is defined by a positive electric potential for containing positively charged particles. We have also chosen to ignore any magnetic interactions internally in the trap, as these will have a small effect compared to the electric interactions.

II. METHODS

A. Finding the equations of motion

To understand the movement of a particle inside the Penning trap, we first examined the force being exerted on it as it passed through the electric $\vec{E}$ and magnetic $\vec{B}$ fields. This force is known as the Lorentz force and is defined as:

$$\vec{F}_L = q\vec{E} + q\vec{v} \times \vec{B} \tag{1}$$

The magnetic field is homogeneous and only imposed in the z-direction, while the electric field is given by the negative gradient of the electric potential, V. Given this, the Lorentz force can be expressed as:

$$\vec{F}_L = q(-\nabla V) + q\dot{\vec{r}} \times B_0\hat{k} \tag{2}$$

where B_0 is the magnitude of the magnetic field, $\hat{k}$ is the unit vector in z-direction and where the velocity is $\vec{v} = \dot{\vec{r}}$.

We considered an ideal Penning trap where the electric potential was defined as

$$V = \frac{V_0}{2d^2}\left(2z^2 - x^2 - y^2\right) \tag{3}$$

[a] Our codes can be found on GitHub https://github.com/cecilmkl/comp_phys/tree/main/project3

where V_0 is the potential applied to the electrodes of the Penning trap, and d is the characteristic dimension. Then, the Lorentz force can be expressed as[1]:

$$\vec{F}_L = -q\frac{V_0}{d^2}(-x\hat{i} - y\hat{j} + 2z\hat{k}) + B_0 q(\dot{y}\hat{i} - \dot{x}\hat{j}) \quad (4)$$

Assuming that the Lorentz force is the only external force acting on the particle, we utilised Newton's second law to get our equations of motion:

$$m\ddot{\vec{r}} = \vec{F}_L \quad (5)$$

$$\ddot{\vec{r}} - \frac{1}{m}\vec{F}_L = 0. \quad (6)$$

If we now insert the expression for the Lorentz force(4) into equation 6, we find:

$$\ddot{\vec{r}} + \frac{qV_0}{md^2}(-x\hat{i} - y\hat{j} + 2z\hat{k}) - \frac{qB_0}{m}(\dot{y}\hat{i} - \dot{x}\hat{j}) = 0. \quad (7)$$

We assumed the particles' charge to be positive, $q > 0$, and identified the two following constants

$$\omega_0 \equiv \frac{qB_0}{m} \qquad \text{and} \qquad \omega_z^2 \equiv \frac{2qV_0}{md^2}$$

Using these constants we rewrote Equation 7 as the following second order differential equations:

$$\ddot{x} - \frac{1}{2}w_z^2 x - w_0\dot{y} = 0, \quad (8)$$

$$\ddot{y} - \frac{1}{2}w_z^2 y + v_0\dot{x} = 0, \quad (9)$$

$$\ddot{z} + w_z^2 z = 0. \quad (10)$$

These equations are the equations of motion for the particle. However, notice that the first two equations(8 and 9) are coupled. This can pose a challenge when it comes to analytically calculating a result, we therefore rewrote these coupled equations as one equation.

B. Rewriting the EOM as a complex function

We introduced a complex function

$$f(t) = x(t) + iy(t) \quad (11)$$

So that the real and imaginary part of the function stores the particles x and y positions respectively. We expressed the derivatives and double derivatives of x and y in terms of this imaginary function, and proceeded to rewrite one of the coupled equations[2]. We found that the other part of the coupled equations emerges, but as it is equal to zero we were left with:

$$\ddot{f} + i\omega_0\dot{f} - \frac{1}{2}\omega_z^2 f = 0, \quad (12)$$

where f is the complex function 11 and $\dot{f}$ and $\ddot{f}$ are the single and double derivatives. The general solution to equation 12 is given by:

$$f(t) = A_+ e^{-i\omega_+ t} + A_- e^{-i\omega_- t} \quad (13)$$

where:

$$\omega_\pm = \frac{\omega_0 \pm \sqrt{\omega_0^2 - 2\omega_z^2}}{2}. \quad (14)$$

C. Constraints on the general solution

It is worth noting that if we let $t \to \infty$, we would end up getting $|f(t)| \to \infty$, therefore we needed to impose some constraints on ω_z and ω_0 to keep $|f(t)| < \infty$ when $t \to \infty$. As ω_0 and ω_z contains the parameters of the Penning trap and the properties of the particle, this also lead to a constraint to the parameters of the Penning trap in relation to the particles properties.

As $\omega_\pm$ can contain an imaginary component(14), we wrote $\omega_\pm$ on the general complex form: $\omega_\pm = a_\pm + ib_\pm$. By inserting this into the general solution(13), we found that the imaginary component of $\omega_\pm$ drove $|f(t)| \to \infty$ as $t \to \infty$[3]. We solved this by demanding that $\omega_\pm$ has no imaginary component, that is, $\omega_\pm \in R$. This applied the following constraints on ω_z and ω_0 as a result of equation 14:

$$\omega_z^2 \leq \frac{1}{2}\omega_0^2, \qquad \omega_0 \in R \quad (15)$$

As previously mentioned ω_z and ω_0 contains the parameters of the Penning trap and the properties of the particle. Therefore, we found another constraint on the penning trap parameters in relation to the particles properties by fully writing out the inequality 15[4]:

$$\frac{4V_0}{d^2 B_0^2} \leq \frac{q}{m}. \quad (16)$$

Where the left hand side of the inequality(16) contains the parameters of the Penning trap, and the right hand side contains the properties of the particle.

---

[1] This expansion/calculation is found in appendix V A, as well as the transition to the differential equations.

[2] How we can rewrite the coupled equations into one complex function is shown in appendix V B

[3] This is shown in appendix V E

[4] The constraints related to ω_0 and ω_z, as well as the one for the properties of the Penning trap are shown more extensively in appendix V E

D. Finding the upper and lower bounds of the particles position in the xy-plane

We further calculated the upper and lower bounds of the particle's distance from the origin in the xy-plane. The distance from the origin in the xy-plane is given by $R = \sqrt{x^2 + y^2}$. We know that the x and y coordinates of the particle can be fetched from the real and imaginary part of function 13 for the position of the particle, so that:

$$x = Re(f(t)) \qquad y = Im(f(t)).$$

By doing this calculation[5] we found that

$$R = \sqrt{A_+^2 + A_-^2 + 2A_+A_- \cos(\omega_+ t - \omega_- t)}. \tag{17}$$

The maximum output value of the cosine function is one and the minimum is minus one. The distance from the origin in the xy-plane is therefore maximized when the cosine function is equal to one, and minimized when it is equal to minus one, yielding the upper and lower bounds:

$$R_- = \sqrt{(A_+ - A_-)^2} = |A_+ - A_-| \tag{18}$$
$$R_+ = \sqrt{(A_+ + A_-)^2} = A_+ + A_- \tag{19}$$

A_+ and A_- can be assumed to be positive, so we don't need the absolute value for the upper boundary R_+(19).

E. Analytical solution

Before implementing a numerical solution and simulation, we first wished to calculate an analytical solution. This allowed us to get a better grasp on how well our simulation is able to estimate the exact result.

First, we already had an expression(13) for the general solution of x and y. From equation 10, we found that the general solution for z[6] is:

$$z(t) = C\cos(w_z t) + iD\sin(w_z t). \tag{20}$$

Where C and D are unknown constants determined by the boundary conditions imposed on z. For our specific solution for $x(t)$, $y(t)$ and $z(t)$ we chose the following values[7]:

$$x(0) = x_0 \qquad \dot{x}(0) = 0$$
$$y(0) = 0 \qquad \dot{y}(0) = v_0$$
$$z(0) = z_0 \qquad \dot{z}(0) = 0.$$

By using these initial conditions for z and $\dot{z}$, we found that $C = z_0$ and $D = 0$ giving the specific solution for z[8]:

$$z(t) = z_0\cos(w_z t). \tag{21}$$

We found the general solution for x and y by expanding the expression for the general solution(13) and utilizing $x = Re(f)$ and $y = Im(f)$, giving us[9]:

$$x(t) = A_+\cos(w_+ t) + A_-\cos(w_- t), \tag{22}$$
$$y(t) = -(A_+\sin(w_+ t) + A_-\sin(w_- t)). \tag{23}$$

By applying the initial conditions for x, y, $\dot{x}$ and $\dot{y}$, we were able to find the expression for A_- and A_+:

$$A_- = -\frac{v_0 + x_0 w_+}{w_- - w_+}, \tag{24}$$
$$A_+ = \frac{x_0 w_- + v_0}{w_- - w_+}. \tag{25}$$

Inserting equations 24 and 25 into equations 22 and 23 yielded the specific solution for $x(t)$ and $y(t)$[10].

F. The algorithm

Algorithm 1 4th order Runge-Kutta method for evolving the penningtrap system one timestep

Here we provide a pseudo code to illustrate how we evolved the system using RK4. The variables are defined as follows: r is the position of a particle, $v = \dot{\vec{r}}$ is the velocity and $a = \ddot{\vec{r}}$ is the acceleration. Furthermore, m is the mass of the particle and h is the step-size.

Input: Add information about chosen step-size h

for every particle in PenningTrap **do**
  if particle is out of bounds **then**
    a = 0
  else
    a = total force on i/m;
  $K_{1r} = h \cdot v(t, x)$;
  $K_{1v} = h \cdot a(t, v)$;
  $K_{2r} = h \cdot v\left(t + \frac{1}{2}h, x + \frac{1}{2}K_1 r\right)$;
  $K_{2v} = h \cdot a\left(t + \frac{1}{2}h, v + \frac{1}{2}K_1 v\right)$;
  $K_{3r} = h \cdot v\left(t + \frac{1}{2}h, x + \frac{1}{2}K_2 r\right)$;
  $K_{3v} = h \cdot a\left(t + \frac{1}{2}h, x + \frac{1}{2}K_2 v\right)$;
  $K_{4r} = h \cdot v(t + h, x + K_3 r)$;
  $K_{4v} = h \cdot a(t + h, x + K_3 v)$;
  $r = r + \frac{1}{6}(k_{1r} + 2K_{2r} + 2K_{3r} + K_{4r})$;
  $v = v + \frac{1}{6}(k_{1v} + 2K_{2v} + 2K_{3v} + K_{4v})$;

[5] How we can write R in terms of $Re(f(t))$ and $Im(f(t))$ is shown in appendix V C

[6] Calculation for the general solution of z is found in appendix V A

[7] This values are also used in our simulation to determine the particles initial conditions, in order to make a comparison between the analytical and numerical solution more relevant.

[8] This is shown in appendix V D

[9] This expansion is shown in appendix V D

[10] The full expressions and calculations are found in V D

Note that the simulation was run with some initial conditions chosen at random. The random numbers produced will vary depending on what machine runs the simulation. As a result of this, you might not get the same exact results if you try to reproduce the data as your initial conditions might be different. However, you can expect to see the same amount of accuracy for the simulation, and can do the same analysis.

III. RESULTS AND DISCUSSION

We chose the following configuration for our Penning trap simulation:

$$d = 10^4 \mu m$$
$$B_0 = 9.65 \cdot 10^1 \frac{u}{(\mu s)e}$$
$$V_0 = 9.65 \cdot 10^8 \frac{u(\mu m)^2}{(\mu s)^2 e}$$

Then, we inserted a singly-charged Ca^+ particle into the Penning trap with the parameters:

$$\vec{r} = x_0\hat{i} + z_0\hat{k} \qquad q = 1\ e$$
$$\vec{v} = v_0\hat{j} \qquad m = 40.078\ u$$

where x_0, y_0 and z_0 were chosen randomly within the boundaries of the trap. We made a plot of the motion in z-direction to compare to the uncoupled analytical solution, $z(t) = z_0 \cos(\omega_z t)$. The result is shown in Figure 1.

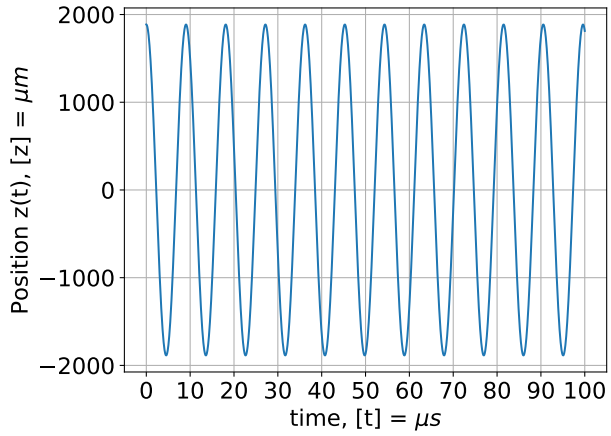

FIG. 1. The figure shows the position of a particle in the z-direction inside the Penning trap as a function of time. The particles position is given in micrometers relative to z(t)=0, and the time ranges from $0\mu s$ to $100\mu s$. The time is sampled 10000 times on the interval, equivalent to a step size of $0.01\mu s$.

Looking at figure 1 we observed a periodic oscillation around $z = 0$, with what seems to be a constant amplitude for the duration of the simulation. The oscillation in the z-direction show what effect the electric field had on the particle, keeping it within the trap in that direction. The particle had a period of around $T = 9\ \mu s$, which corresponds to the analytical period of $T = \frac{2\pi}{|\omega_z|} = 9.05\ \mu s$. Furthermore, the analytical solution oscillates with amplitude $z_0 = z(0)$, which our simulation seems to do as well. This indicates that our approximation to the Penning trap system might be sufficient.

Then, we added a second particle, also a Ca^+ ion, into our system, and gave it a random position and velocity scaled to the size of our trap. We made a plot of their movement in the xy-plane when we neglected interactions between the particles and when we accounted for them. The result is presented in figure 2. We expected the particles to have orbital motions due to the magnetic field imposed in the z-direction. For easy comparison, we made sure to keep the initial conditions for both particles the same with and without interactions in all our simulations.

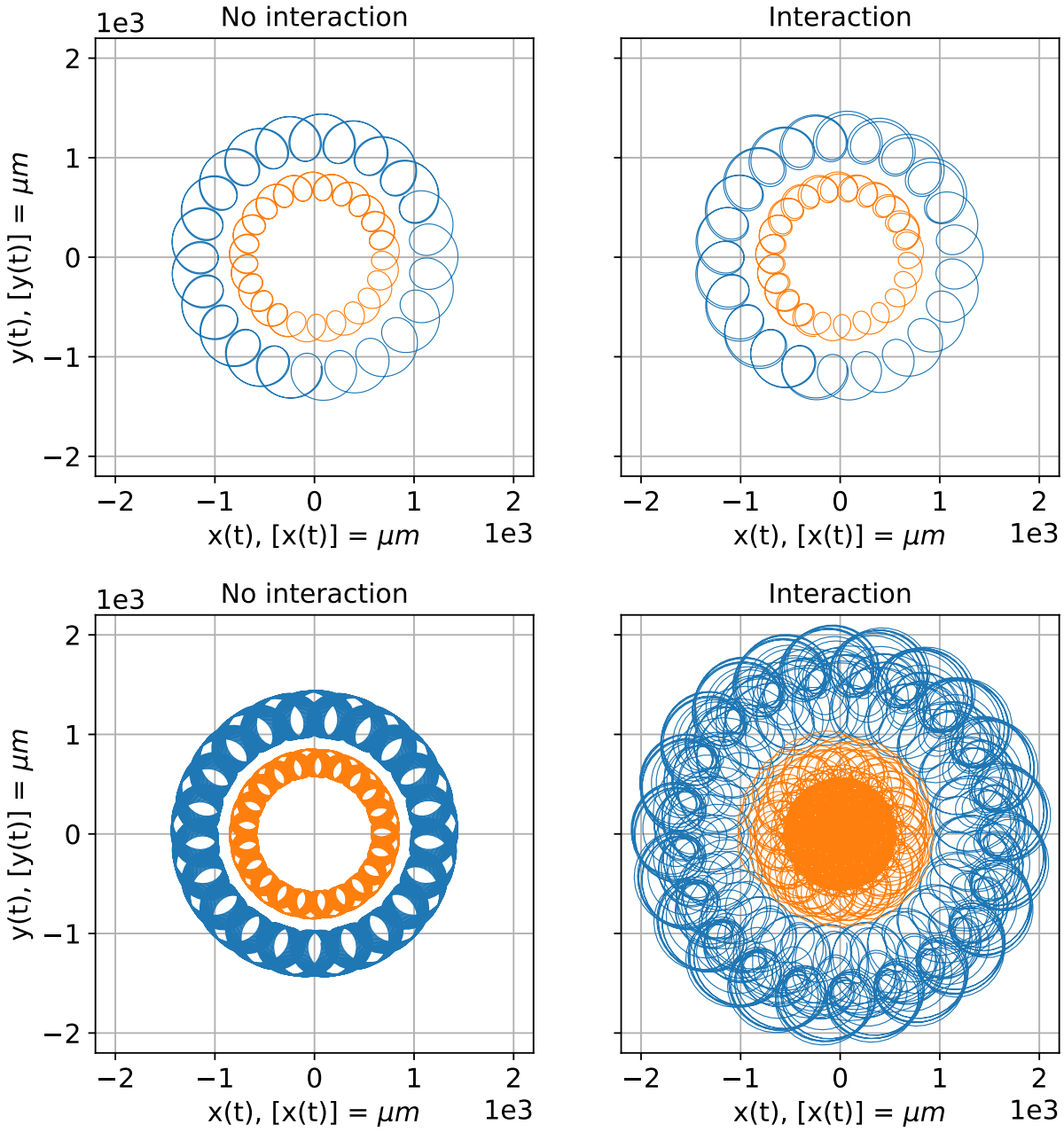

FIG. 2. This figure displays the behaviour of two particles when particle interactions are neglected (left) and when they are included (right), with the same initial starting positions and velocities. The motion is shown after 100 μs (top) and after 1000 μs (bottom), where the effect is more noticeable.

Figure 2 illustrates the difference including inter-particle interactions make. We see the expected effect of the magnetic field, as it forces the particles into an orbit when moving through the field hindering them from escaping the trap. The case of no interaction seems to have a stable periodic path based on their start positions and velocities. When interactions were accounted for, the particles were displaced into different orbits further out and further in respectively until they reached a stable orbit. This is because the interactions between the particles will push the outer particle further away from the centre, whilst the innermost is pushed toward the centre. This effect is due to the particles repelling each other, since their charge is the same.

The effect of inter-particle interactions were further explored by plotting the motion of each particle in the 3-dimensional xyz-space. Figure 3 shows the particles with interactions turned off (left) and on (right). We included two timescales to better see single pathways (top) and closer to the stable orbit (bottom).

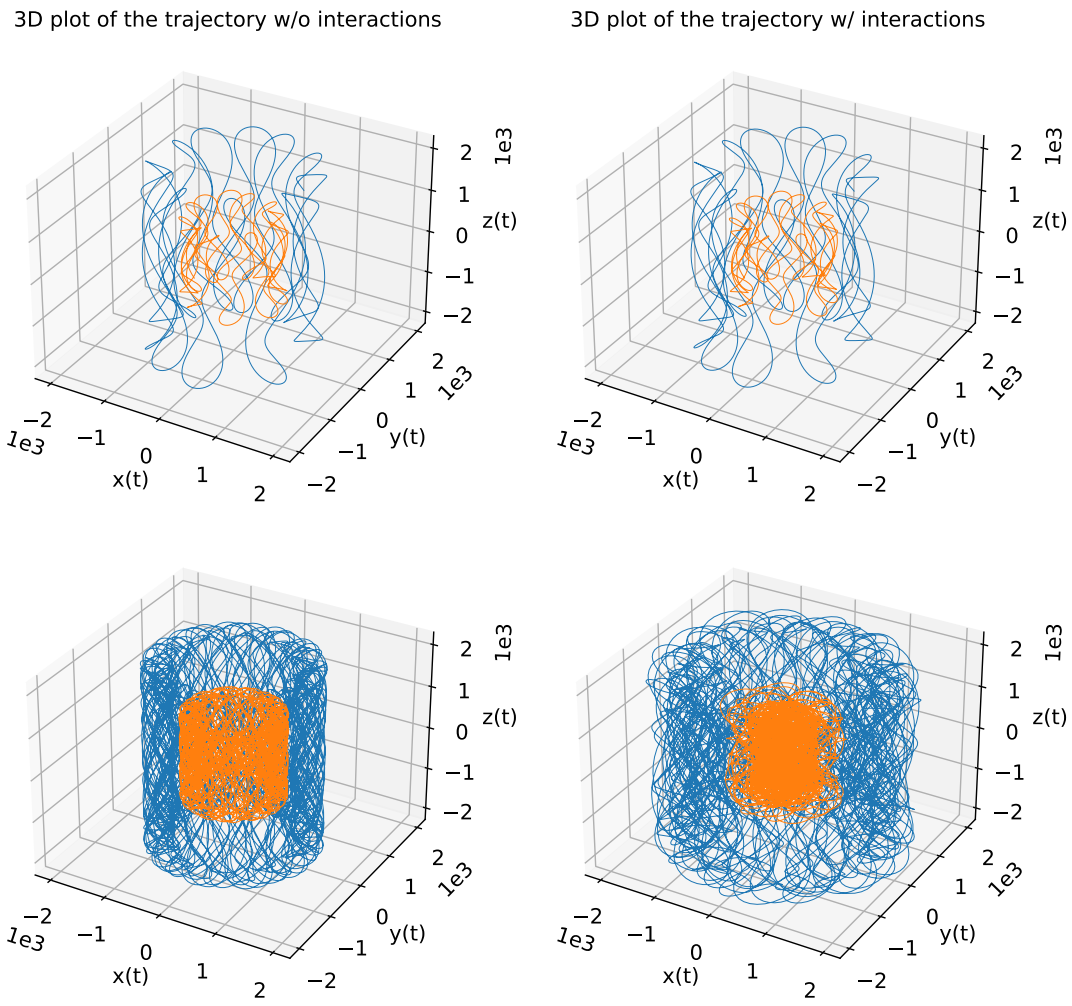

FIG. 3. This plot shows the two paths taken by the two particles over the time interval $t = [0\mu s, 100\mu s]$ with a time step of $0.01\mu s$, when there is no interactions (left), with interactions (right), after time 100 μs (top) and 1000 μs (bottom).

In Figure 3 both particles seemingly move periodically in z-direction, in accordance with what we observed in Figure 1. This was due to the electric field restraining motion in the z-direction. We also see that the particles chose paths that had different distances from the origin depending on their initial conditions, which corresponds to what we saw in Figure 2.

The particles move as expected due to the Lorentz force being the only force effecting the particles and causing a repeating pattern in the motion of each particle. As energy is conserved in this case, we expect to see a repeating pattern in the no-interactions case.

We see that when we included interactions in our simulation, the movement became more chaotic, due to the effects the particles have on each other. The particles still remained within the trap, however they moved further away from their original orbits. The other particle is pushed to move further out, and the innermost one closer in, like we saw in Figure 2. This is clearer to see in the simulation taken over a longer time-period. We observe here a new equilibrium with the outer particle occupying a broader area, and the innermost spending more time closer to the centre. Due to their different energies in these stages, a collision is unlikely to make them switch places, as the outermost particle would have enough energy to move further out again, and the innermost is unlikely to.

It is worth noting here however, the limitations of simulations as opposed to reality. If particle A is evolved before a particle B, A will, in the next time step, have a position further away from B when the Coulomb force is calculated for B. This will cause particle A and y to experience different forces, which violates Newton's third law of motion as the two are opposing forces. Additionally, this would cause an unreasonably large Coulomb force, potentially giving the second particle enough energy to escape. We have chosen therefore to make such collisions impossible, but it would be a potential contributor to inaccuracies for especially large step-sizes.

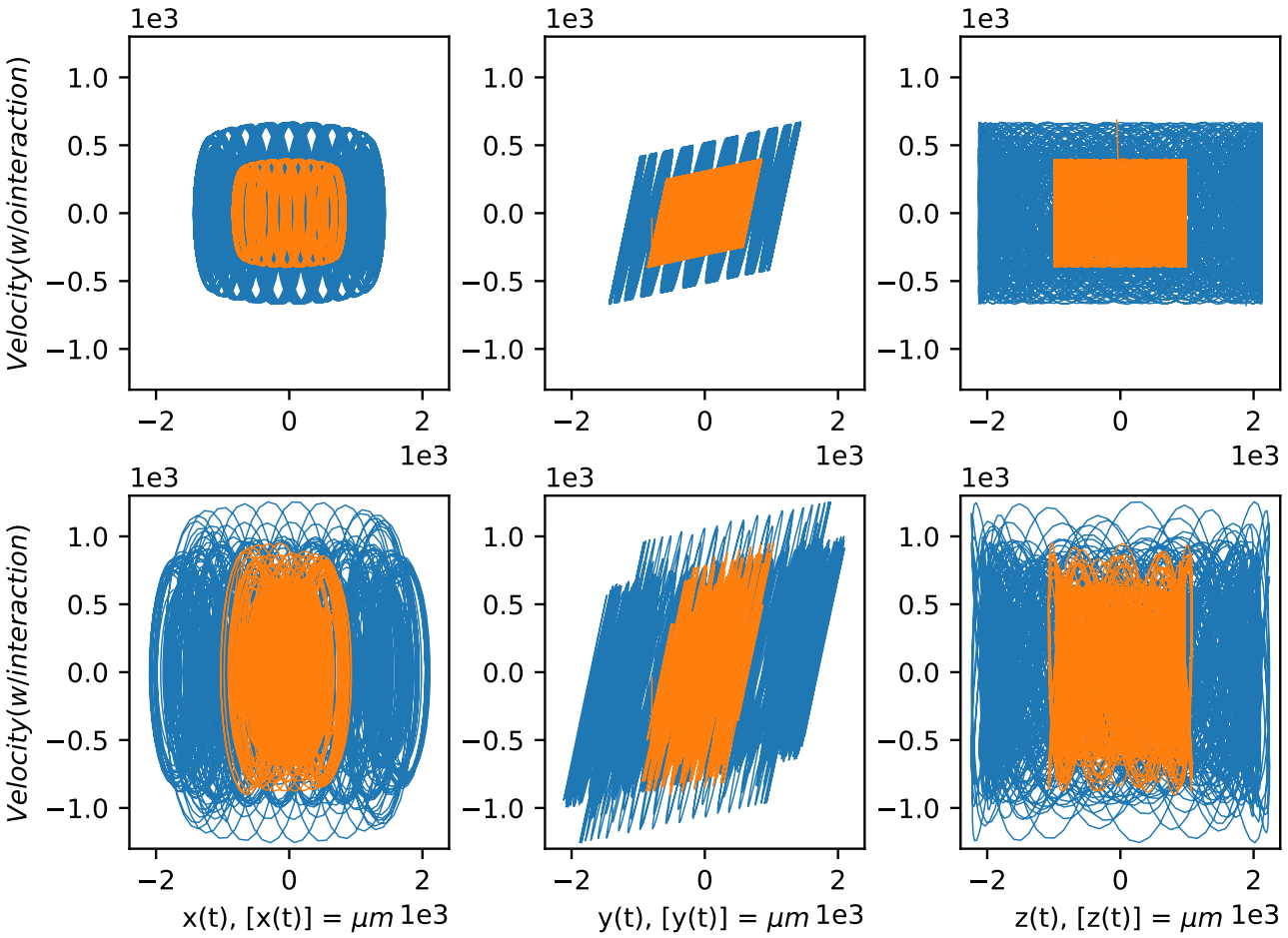

FIG. 4. This figure shows the various phase-space plots for time-step $h = 0.1\mu s$ for total time $1000\mu s$. From left to right it shows: x vs. v_x, y vs. v_y, z vs. v_z. The top row has the simulations without particle interactions, the bottom row includes particle interactions.

Figure 4 gives the various phase-space plots in each direction. All three directions illustrate the oscillatory effects as expected, due to the magnetic influence over the x-, and y-directions, and electric influence in the z-direction. We also observe the same effects in directional space as seen earlier, with the outer particle occupying a larger space when interactions are included, and the innermost particle spending more time in the centre. In a similar way, the velocity increases for both particles when interactions are included. So we can see that both the directional movement, and the velocities has more overlap with interactions, the movement is more chaotic while still having oscillatory trends, and their movements occupy a bigger range of paths and velocities.

We would expect, comparing this to figure 3, that the plots in the x-direction and y-direction, but for reasons we are unable to deduce, this is not the case in figure 4.

A. Error analysis

In order to get an impression of how well our simulation did, we had to perform an error analysis. First we wanted to plot the relative error for different step-sizes. We calculated the relative error the following way:

$$r_{rel} = \left| \frac{\vec{r}_{estimated} - \vec{r}_{exact}}{\vec{r}_{exact}} \right|. \tag{26}$$

Where $\vec{r}$ is the position vector of the particle. The estimated position vector is the position calculated by our simulation. By setting the initial conditions of our simulation equal to the ones outlined in section II E, our analytical solution in section II E provides the exact position of the particle.

By using these values we could generate the following plot of the relative error across different step sizes for the Euler-Cromer method:

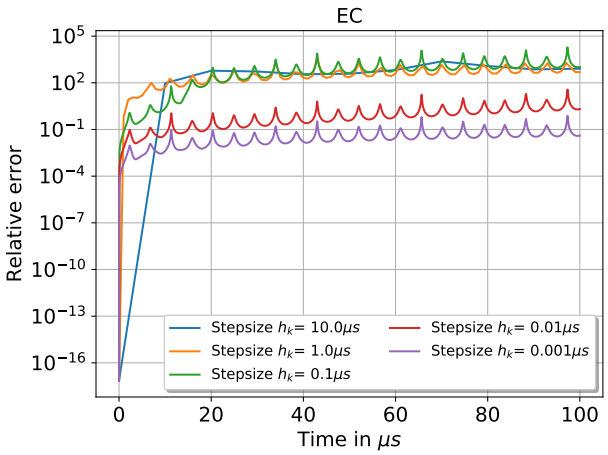

FIG. 5. The plot shows the relative error(logarithmic scale) for different step sizes, when using Euler-Cromer to calculate the position of the particle.

Figure 5 shows that the simulation clearly lacks precision, especially for larger step sizes. The smallest step-size of $h_k = 0.001\mu s$ gives a relative error of about 0.1, towards the end of the simulation, which is not ideal.

As the 4th order Runge-Kutta method we used is more precise, although more costly, we find it interesting to compare the two. The relative error of using the Runge-Kutta method is shown below:

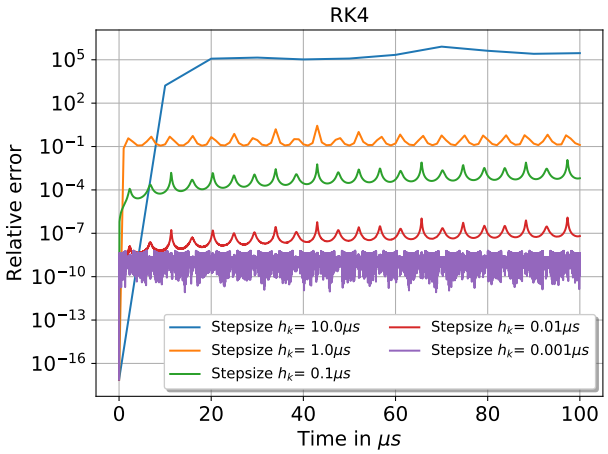

FIG. 6. The plot shows the relative error(logarithmic scale) for different step-sizes, when using the 4th order Runge-Kutta method.

Figure 6 clearly shows an improvement in the relative error compared to figure 5. We can see that a step-size of $h_k = 0.1\mu s$ using the Runge-Kutta actually provides a smaller relative error than a step-size of $h_k = 0.001\mu s$ using Euler-Cromer.

It is worth noting that figure 6 shows some weird behavior for $h_k = 0.001\mu s$. We are not sure what exactly causes this behavior, but it might be a consequence of how many decimals we choice to include when we saved data from the simulation. As the the exact solution is calculated using the time-steps from the simulation, but is not rounded to the same number as the estimated position values, we could see a small remainder in r_{rel} for each time-step. This could be an explanation for the volatile behavior we see for $h_k = 0.001\mu s$ in figure 6.

Figure 5 shows that the approximation done by Euler-Cromer only marginally improves for each reduction of the time-step. Figure 6 however, shows that the relative error by Runge-Kutta drastically improves for each time-step(note that the scale of the plots y-axis is logarithmic.). This is also reflected in the error convergence rate of the two methods:

Method	Error Convergence Rate
Euler-Cromer	1.0754520814311255
Runge-Kutta 4	3.4547661718627385

TABLE I. This table shows the calculated error convergence rates for both methods.

We calculated the error convergence rates in table I by using the expression:

$$r_{err} = \frac{1}{4}\sum_{k=2}^{5}\frac{\log(\Delta_{max,k}/\Delta_{max,k-1})}{\log(h_k/h_{k-1})} \tag{27}$$

After we explored the basics of our Penning trap, we proceeded to investigate the possibility of seeing resonance phenomena by subjecting the system to a time-dependant electric field. We achieved this by including a time-dependant perturbation to the applied potential,

$$V_0 \to V_0(1 + f\cos(\omega_V t)),$$

where f is a constant amplitude and ω_V is the angular frequency.

The aim was to search for resonance frequencies of the system and to investigate if the Coulomb interactions have an impact on the resonance structures. We decreased the size of our Penning trap as well as the initial applied electric potential V_0 in an effort to increase the possibility to observe resonance phenomena. The magnetic field was kept the same as before such that the new configuration was as follows:

$$d = 500\mu m$$
$$V_0 = 2.412 \cdot 10^5 \frac{u(\mu m)^2}{(\mu s)^2 e}$$

We filled our Penning trap with 100 Ca^+ ions with the same charge and mass as before, and gave them random positions and velocities scaled to our trap. We turned off the particle interactions to get a better run-time for our

code. Then, we ran experiments on the system for applied angular frequencies $\omega_V \in (0.2, 2.5)MHz$ where we counted the remaining particles after $500\mu s$. We chose a step-size of $0.01MHz$ and repeated the experiments for different amplitudes, $f = 0.1, 0.4, 0.7$. The result is shown in Figure 7, where the fraction of remaining particles are plotted as a function of the applied angular frequency, ω_V.

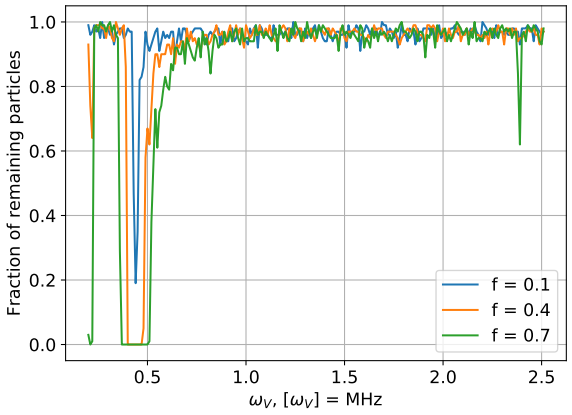

FIG. 7. This plot shows the relation between the applied angular frequency ω_V, and the fraction of particles that remain in the Penning trap when the electric potential has applied amplitude $f = 0.1$, $f = 0.4$ and $f = 0.7$

.

To get a better understanding of the resonance spike at around $\omega_V = 0.45$, we "zoomed in" by performing a fine-grained frequency scans around it. We chose to examine the interval $\omega_V \in (0.3, 0.6)$ that is shown in 8 using an amplitude of f = 0.1.

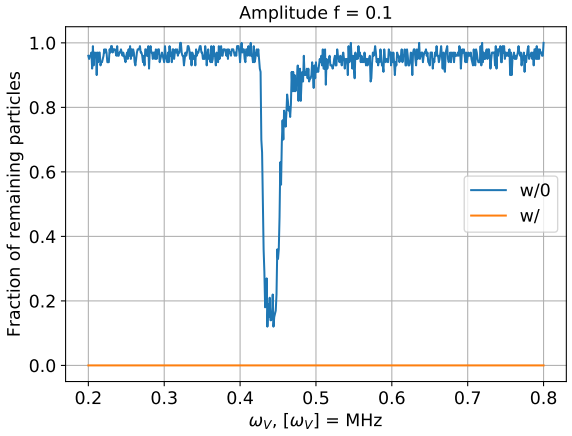

FIG. 8. The plot shows the result of fine-grained frequency scans around the resonance at frequency $\omega_V \approx 0.44$. The blue line is the scan without Coulomb interactions, while the orange line is the scan with Coulomb interactions.

This effect is caused when the applied frequency closely match the internal frequency of the particles. When this happens, the oscillatory amplitudes are greatly increased, and have the potential to give them energy to escape the forces keeping them inside the trap. This provides us with a method to find resonance frequencies as a function between applied frequency and number of remaining particles. A larger amplitude to the applied angular frequency will give more energy to the particle oscillations, causing a larger internal amplitude increase. Hence we observe more particles escaping. Furthermore, we know from the values of the internal $\omega_{z,+,-}$ given in section II A and II B, that the frequencies will depend on the external fields, and the masses. This we observe in the code, by the fact that changing either of these values, we obtain different resonance frequencies.

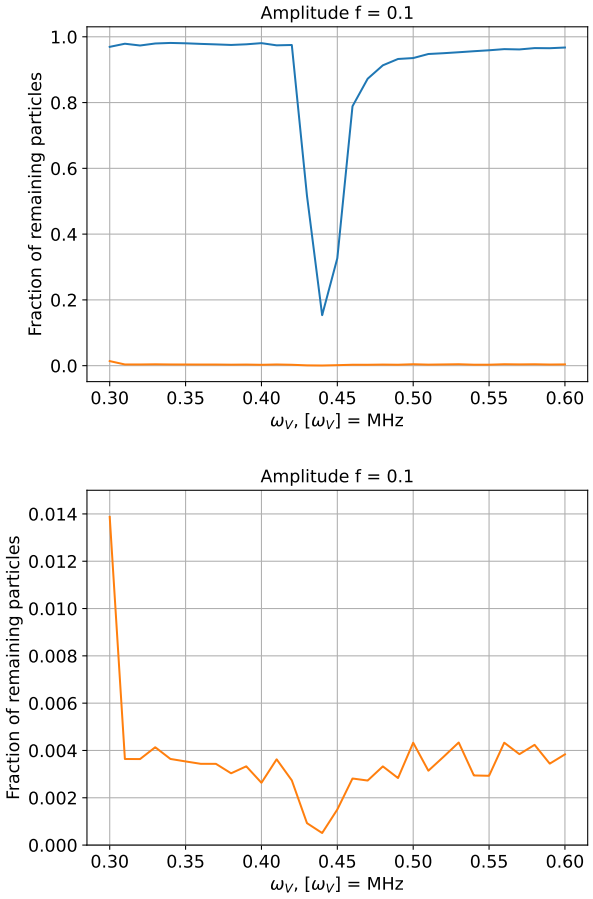

FIG. 9. The same scan as in 8, less fine grained but averaged over 100 runs. The Bottom plot is zoomed in on the scan with particle interactions.

IV. CONCLUSION

This research has produced a numerical simulation of a Penning trap using the 4th order Runge-Kutta algorithm. By analysing the particle equations of motion due

to the external fields, we have concluded that our simulation successfully exhibit the oscillatory effects expected. Furthermore, we have shown the effects inter-particle interactions have on the system, and what applied external frequencies will cause the most particles to escape the trap. In comparison to the Euler-Cromer method we found our relative errors to be substantially less, justifying the less effective Runge-Kutta method.

[1] Butcher, J. (2003). *Numerical Methods for Ordinary Differential Equations*. John Wiley & Sons.
[2] Huang, W. X. et al. (2013). Status of Lanzhou Penning Trap for accurate mass measurements. *Nucl. Instrum. Meth. A*, 317:528–531.

V. APPENDIX

A. Obtaining particle equation of motion

Starting from Newton's second law:

$$m\ddot{\vec{r}} = \sum_i \vec{F}_i^{\,ext}$$
$$\ddot{\vec{r}} - \frac{1}{m}\sum_i \vec{F}_i^{\,ext} = 0$$

Then using Lorentz force:

$$\ddot{\vec{r}} - \frac{1}{m}(q\vec{E} + q\dot{\vec{r}} \times \vec{B}) = 0$$
$$\ddot{\vec{r}} - \frac{1}{m}(q(-\boldsymbol{\nabla} V) + q\dot{\vec{r}} \times B_0\hat{k}) = 0$$

with:

$$\begin{aligned}
\boldsymbol{\nabla} V &= \left[\hat{i}\frac{\delta}{\delta x} + \hat{j}\frac{\delta}{\delta y} + \hat{k}\frac{\delta}{\delta z}\right]\left(\frac{V_0}{2d^2}\left(2z^2 - x^2 - y^2\right)\right) \\
&= \frac{V_0}{2d^2}\left[\hat{i}\frac{\delta}{\delta x}\left(-x^2\right) + \hat{j}\frac{\delta}{\delta y}\left(-y^2\right) + \hat{k}\frac{\delta}{\delta z}\left(2z^2\right)\right] \\
&= \frac{V_0}{2d^2}\left[\hat{i}(-2x) + \hat{j}(-2y) + \hat{k}(4z)\right] \\
&= \frac{V_0}{d^2}\left(-x\hat{i} - y\hat{j} + 2z\hat{k}\right),
\end{aligned}$$

and

$$\begin{aligned}
q\dot{\vec{r}} \times B_0\hat{k} &= q\left(\dot{\vec{r}} \times B_0\hat{k}\right) \\
&= q\begin{vmatrix} \hat{i} & \hat{j} & \hat{k} \\ \dot{x} & \dot{y} & \dot{z} \\ 0 & 0 & B_o \end{vmatrix} \\
&= q\left[\hat{i}\left(\dot{y}B_0\right) - \hat{j}\left(\dot{x}B_0\right) + \hat{k}(0)\right] \\
&= B_0 q\left(\dot{y}\hat{i} - \dot{x}\hat{j}\right) \\
&= B_0 q\dot{y}\hat{i} - B_0 q\dot{x}\hat{j} \\
&= \left(B_0 q\dot{y}, -B_0 q\dot{x}, 0\right).
\end{aligned}$$

Going back to Newton's second law:

$$\ddot{\vec{r}} - \frac{1}{m}\left[q(-\boldsymbol{\nabla} V) + \left(q\ddot{\vec{r}} \times B_0\hat{k}\right)\right] = 0$$
$$\ddot{\vec{r}} - \frac{1}{m}q\left(-\frac{V_0}{d^2}\left(-x\hat{i} - y\hat{j} + 2z\hat{k}\right)\right) - \frac{B_0}{m}q\left(\dot{y}\hat{i} - \dot{x}\hat{j}\right) = 0$$
$$\dot{\vec{r}} - \frac{1}{m}q\frac{V_0}{d^2}\left(x\hat{i} + y\hat{j} - 2z\hat{k}\right) - \frac{B_0}{m}q\left(\dot{y}\hat{i} - \dot{x}\hat{j}\right) = 0.$$

We then rewrite $\frac{1}{m}q\frac{V_0}{d^2} = \frac{1}{2}w_z^2$ and $\frac{B_0}{m}q = w_0$, and the equation can then be decomposed to:

$$\begin{aligned}
&\ddot{x} - \frac{1}{2}w_z^2 x - w_0\dot{y} = 0 \\
&\ddot{y} - \frac{1}{2}w_z^2 y - v_0\dot{x} = 0 \\
&\ddot{z} - \frac{1}{2}w_z^2(-2z) = \ddot{z} + w_z^2 z = 0.
\end{aligned}$$

From this we obtain a general solution for $\ddot{z} + w_z^2 z = 0$ with $z = e^{rt}$, $\dot{z} = re^{rt}$ and $\ddot{z} = r^2 e^{rt}$, so that:

$$\begin{aligned}
&r^2 e^{rt} + w_z^2 e^{rt} = 0 \\
&e^{rt}\left(r^2 + w_z^2\right) = 0 \\
&r^2 + w_z^2 = 0 \\
&r^2 = -w_z^2 \\
&r = \pm\sqrt{-w_z^2} = \pm i w_z.
\end{aligned}$$

Which gives:

$$\begin{aligned}
z(t) &= Ae^{iw_z t} + Be^{-iw_z t} \\
&= A\left(\cos(w_z t) + i\sin(w_z t)\right) + B\left(\cos(-w_z t) + i\sin(-w_z t)\right) \\
&= A\left(\cos(w_z t) + i\sin(w_z t)\right) + B\left(\cos(w_z t) - i\sin(w_z t)\right) \\
&= (A+B)\cos(w_z t) + i\,(A-B)\sin(w_z t),
\end{aligned}$$

Then using new constants: $C = A + B$ and $D = A - B$ we obtain:

$$z(t) = C\cos(w_z t) + iD\sin(w_z t). \tag{28}$$

B. Rewriting as a complex function

We have the two differential equations for the motion of the particle:

$$\ddot{x} - \omega_0 \dot{y} - \frac{1}{2}\omega_z^2 x = 0 \tag{29}$$

$$\ddot{y} + \omega_0 \dot{x} - \frac{1}{2}\omega_z^2 y = 0 \tag{30}$$

Assuming we have a complex function $f(t) = x(t) + iy(t)$, the functions derivative, and double derivative can be written as follows:

$$f = x + iy \qquad \dot{f} = \dot{x} + i\dot{y} \qquad \ddot{f} = \ddot{x} + i\ddot{y}$$

Which can be rewritten as:

$$x = f - yi \qquad \dot{y} = i(\dot{x} - \dot{f}) \qquad \ddot{x} = \ddot{f} - \ddot{y}i$$

Inserting this into the "first" differential equation 29, we get:

$$\ddot{f} - i\ddot{y} - \omega i(\dot{x} - \dot{f}) - \frac{1}{2}\omega_z^2(f - iy) = 0$$

$$\ddot{f} + \omega_0 i\dot{f} - \frac{1}{2}\omega_z^2 f \underline{- i\ddot{y} - \omega_0 i\dot{x} + \frac{1}{2}\omega_z^2 iy} = 0$$

We identify the underlined part above as the other coupled differential equation 30 multiplied with $-i$, that is:

$$\ddot{y} + \omega_0 \dot{x} - \frac{1}{2}\omega_z^2 y = 0 \xrightarrow{\cdot(-i)} -i\ddot{y} - \omega_0 i\dot{x} + \frac{1}{2}\omega_z^2 iy = 0$$

We are then left with:

$$\ddot{f} + \omega_0 i\dot{f} - \frac{1}{2}\omega_z^2 f = 0 \tag{31}$$

In other words, the coupled differential equations 29 and 30 are written as 31, where f is the complex function $f(t) = x(t) + iy(t)$.

C. Particles distance from origin

We have the general solution of the particles position:

$$f(t) = A_+ e^{-i\omega_+ t} + A_- e^{-i\omega_- t}$$

We know the distance from the origin in the xy-plane is given by

$$R = \sqrt{x^2 + y^2}$$

Since we know that ω_+ and ω_- are real numbers(15) we find that x and y can be written as:

$$\begin{aligned}
x &= Re(f(t)) = A_+ \cos(\omega_+ t) + A_- \cos(\omega_- t) \\
y &= Im(f(t)) = -A_+ \sin(\omega_+ t) - A_- \sin(\omega_- t) \\
x^2 &= A_+^2 \cos^2(\omega_+ t) + 2A_+ A_- \cos(\omega_+ t)\cos(\omega_- t) + A_-^2 \cos^2(\omega_- t) \\
y^2 &= A_+^2 \sin^2(\omega_+ t) + 2A_+ A_- \sin(\omega_+ t)\sin(\omega_- t) + A_-^2 \sin^2(\omega_- t)
\end{aligned}$$

We then have:

$$\begin{aligned}
R &= \sqrt{x^2 + y^2} \\
&= \sqrt{A_+^2(\cos^2(\omega_+ t) + \sin^2(\omega_+ t) + 2A_+ A_-(\cos(\omega_+ t)\cos(\omega_- t) + \sin(\omega_+ t)\sin(\omega_- t)) + A_-^2(\cos^2(\omega_- t) + \sin^2(\omega_- t)} \\
&= \sqrt{A_+^2 + A_-^2 + 2A_+ A_- \cos(\omega_+ t - \omega_- t)}
\end{aligned}$$

We know that the $\cos(x)$ can produce a maximum value of 1 and a minimum value of -1. We exploit this fact to find the upper and lower bounds of the particles distance from the origin:

$$\begin{aligned}
R_- &= \sqrt{A_+^2 + A_-^2 - 2A_+ A_-} = \sqrt{(A_+ - A_-)^2} = |A_+ - A_-| \\
R_+ &= \sqrt{A_+^2 + A_-^2 + 2A_+ A_-} = \sqrt{(A_+ + A_-)^2} = |A_+ + A_-|
\end{aligned}$$

Note that if both A_+ and A_- are positive we simply have:

$$R_+ = A_+ + A_-$$

Where R_- represents the lower boundary of the particles distance from the origin in the xy-plane, and R_+ represents the upper boundary.

D. Obtaining specific solution to $z(t)$ and $f(t)$

To find the specific solution to $z(t)$ we start from the general solution given in Equation 28. We also use the initial conditions of:

$$\begin{aligned} x(0) &= x_0 & \dot{x}(0) &= 0 \\ y(0) &= 0 & \dot{y}(0) &= v_0 \\ z(0) &= z_0 & \dot{z}(0) &= 0. \end{aligned}$$

We begin by finding the first derivative $\dot{z}(t)$

$$\begin{aligned} \dot{z}(t) = \frac{d}{dt}z(t) &= C\left(-w_z \sin(w_z t)\right) + iD\left(w_z \cos(w_z t)\right) \\ &= -Cw_z \sin(w_z t) + iDw_z \cos(w_z t), \end{aligned}$$

and we apply the initial conditions above to solve for the constants:

$$\begin{aligned} &z(0) = C\cos(w_z \cdot 0) + iD\sin(w_z \cdot 0) = z_0 \\ &C \cdot 1 + iD \cdot 0 = z_0 \\ &\therefore C = z_0, \end{aligned}$$

$$\begin{aligned} &\dot{z}(0) = -Cw_z \sin(w_z \cdot 0) + iDw_z \cos(w_z \cdot 0) = 0 \\ &- Cw_z \cdot 0 + iDw_z \cdot 1 = 0 \\ &iDw_z = 0 \\ &\therefore D = 0. \end{aligned}$$

Applying these to Equation 28 we obtain:

$$z(t) = z_0 \cos(w_z t). \tag{32}$$

To find the specific solution to $f(t)$ we start from the general solution given in Equation 13, and expand using sin and cosine:

$$\begin{aligned} f(t) &= A_+\left(\cos(w_+ t) + i\sin(-w_+ t)\right) + A_-\left(\cos(w_- t) + i\sin(-w_- t)\right) \\ &= A_+\left(\cos(w_+ t) - i\sin(w_+ t)\right) + A_-\left(\cos(w_- t) - i\sin(w_- t)\right) \\ &= \underline{A_+\cos(w_+ t) + A_-\cos(w_- t)} - i\underline{(A_+\sin(w_+ t) + A_-\sin(w_- t))}. \end{aligned}$$

Looking at Equation 11, we can see that the underlined parts can represent $x(t)$ and $y(t)$ as:

$$x(t) = A_+\cos(w_+ t) + A_-\cos(w_- t) \tag{33}$$
$$y(t) = -(A_+\sin(w_+ t) + A_-\sin(w_- t)), \tag{34}$$

which we then apply the given initial conditions to, and solve as simultaneous equations to obtain A_+ and A_-:

$$
\begin{aligned}
& x(0) = A_+ \cos(0) + A_- \cos(0) = x_0 \\
\text{(I)} \quad & A_+ + A_- = x_0
\end{aligned}
$$

$$
\begin{aligned}
& \dot{y}(0) = -A_+ w_+ \cos(w_+ \cdot 0) - A_- w_- \cos(w_- \cdot 0) = v_0 \\
\text{(II)} \quad & -A_+ w_+ - A_- w_- = v_0 \\
& -A_- w_- = v_0 + A_+ w_+ \\
& A_- = \frac{-(v_0 + A_+ w_+)}{w_-}
\end{aligned}
$$

$$
\begin{aligned}
\text{(I)} \quad & A_+ = x_0 - A_- \\
& A_+ = x_0 + \frac{v_0 + A_+ w_+}{w_-} \\
& A_+ w_- = x_0 w_- + v_0 + A_+ w_+ \\
& A_+ (w_- - w_+) = x_0 w_- + v_0 \\
& \underline{A_+ = \frac{x_0 w_- + v_0}{w_- - w_+}}
\end{aligned}
$$

$$
\begin{aligned}
\text{(I)} \quad & A_- = x_0 - A_+ \\
& A_- = x_0 - \frac{x_0 w_- + v_0}{w_- - w_+} \\
& A_- = \frac{x_0 (w_- - w_+) - (x_0 w_- + v_0)}{w_- - w_+} \\
& \underline{A_- = -\frac{v_0 + x_0 w_+}{w_- - w_+}}.
\end{aligned}
$$

These are then added to the equations for $x(t)$ and $y(t)$ from Equation 33 and 34:

$$x(t) = \frac{x_0 w_- + v_0}{w_- - w_+} \cos(w_+ t) - \frac{v_0 + x_0 w_+}{w_- - w_+} \cos(w_- t) \tag{35}$$

$$y(t) = \frac{x_0 w_- + v_0}{w_- - w_+} \sin(w_+ t) - \frac{v_0 + x_0 w_+}{w_- - w_+} \sin(w_- t). \tag{36}$$

E. Constraints of the general solution

We have the general solution:

$$f(t) = A_+ e^{-i\omega_+ t} + A_- e^{-i\omega_- t}.$$

where:

$$\omega_\pm = \frac{\omega_0 \pm \sqrt{\omega_0^2 - 2\omega_z^2}}{2}.$$

And $\omega_0 = \frac{1}{m}(qB_0)$, $\omega_z = \sqrt{\frac{2qV_0}{md^2}}$

To find the necessary constraints on ω_0 and ω_0 to obtain a bounded solution for the particles movement in the xy-plane, we want to find the constraints that uphold $|f(t)| < \infty$ for $t \to \infty$.

$\omega_\pm$ might have an imaginary component, so we introduce the following expression for $\omega_\pm$:

$$\omega_\pm = a_\pm \pm ib_\pm$$

By introducing this expression for $\omega_\pm$ into the general solution, we find:

$$\begin{aligned} f(t) &= A_+ e^{-i(a_+ + ib_+)t} + A_- e^{-i(a_- - ib_-)t} \\ &= A_+ e^{-ia_+ t} e^{-i^2 b_+ t} + A_- e^{-ia_- t} e^{-i^2 b_- t} \\ &= A_+ e^{-ia_+ t} e^{b_+ t} + A_- e^{-ia_- t} e^{b_- t} \end{aligned}$$

for $t \to \infty$:

$$e^{-ict} \in [-1, 1] \text{ for all constants } c \in R,\ e^{b_+ t} \to \infty \text{ and } e^{b_- t} \to \infty$$

we therefor need to limit the contribution form $e^{b_\pm t}$ to keep $|f(t)| < \infty$ when $t \to \infty$. We can do this by setting $b_\pm = 0$ so that:

$$e^{b_\pm t} = e^0 = 1 \text{ for all t}$$

The implication of this is that $\omega_\pm \in R$ since $b_\pm$ represents the imaginary element of $\omega_\pm$.

$$\omega_\pm = \frac{\omega_0 \pm \sqrt{\omega_0^2 - 2\omega_z^2}}{2} \in R$$

Which implies that $\omega_0 \in R$ and we get the following constraints for ω_z and the Penning trap parameters:

$$\begin{aligned} &\sqrt{\omega_0^2 - 2\omega_z^2} \in R \\ \Rightarrow\ &\omega_0^2 - 2\omega_z^2 \geq 0 \\ &\omega_z^2 \leq \frac{1}{2}\omega_0^2 \qquad (37) \\ &\frac{2qV_0}{md^2} \leq \frac{q^2 B_0^2}{2m^2} \\ &\Downarrow q > 0 \\ &\frac{2V_0}{d^2} \leq \frac{qB_0^2}{2m} \\ &\frac{4V_0}{d^2 B_0^2} \leq \frac{q}{m} \qquad (38) \end{aligned}$$

Where line 37 shows the limitations of ω_z and line 38 shows the constraints related to the Penning trap parameters to the particles properties. In other words we have the following constraints:

$$\omega_0 \in R, \qquad \omega_z^2 \leq \frac{1}{2}\omega_0^2, \qquad \frac{4V_0}{d^2 B_0^2} \leq \frac{q}{m}.$$